Energy Reports 12 (2024) 2077–2085

Contents lists available at ScienceDirect

Energy Reports

journal homepage: www.elsevier.com/locate/egyr

Research paper

Deep learning-based evaluation of photovoltaic power generation

Sayawu Yakubu Diaba [a,*], Andrew Adewale Alola [b], Marcelo Godoy Simoes [c], Mohammed Elmusrati [a]

[a] Department of Telecommunications Engineering, School of Technology and Innovations, University of Vaasa, Vaasa, Finland
[b] Department of Business Administration, Inland Norway University of Applied Sciences, Inland, Norway
[c] Department of Electrical Engineering, School of Technology and Innovations, University of Vaasa, Vaasa, Finland

ARTICLE INFO

Keywords:
Distributed generation
Electric power
Green house emission
Power management
Renewable energy resource

ABSTRACT

Photovoltaic (PV) power generation has emerged as a rapidly growing renewable energy source. However, the PV system output's intermittent and weather-dependent nature poses challenges when integrating with the power grid. These challenges manifest as critical issues, including voltage fluctuations, harmonic distortion, and current deviation, making it difficult to accurately predict grid conditions. Moreover, the spatial variability caused by PV system intermittency further complicates the situation. To address these challenges and ensure efficient grid integration, this paper proposes a comprehensive approach encompassing deep learning-based state prediction of PV power output. The paper introduces the utilization of a long short-term memory (LSTM) model, a type of deep learning architecture, for learning patterns from historical PV power generation data and weather forecasts. The LSTM model enables accurate predictions for effective grid management by capturing long-term dependencies in PV power generation data. Real-world PV power generation data was employed to evaluate the proposed approach. The results demonstrated the significant improvement in PV power generation prediction accuracy achieved by the LSTM model compared to traditional methods. The proposed approach offers a promising solution for addressing the challenges associated with PV system integration into the power grid. It enables enhanced grid planning, resource allocation, and protection measures to accommodate the increasing penetration of solar energy harnessed through PV systems and related power electronics interfaces.

1. Introduction

Alternative energy sources, especially renewables, are considered among the best options for driving energy efficiency and the 2050 carbon-zero agenda. Since the development of the first practical PV cell in the early 1950s, advancement in technology, and decline in the cost of PV systems and installations over time alongside financial incentives as provided by governments across the globe, there has been a continuous expansion in the use of the PV for power generation. According to the report of the International Energy Agency (IEA), an increase of 23 % in solar PV generation was recorded in 2020 (International Energy Agency, 2022), thus accounting for the second-largest growth in power generation among all renewable technologies (Kruitwagen et al., 2021). Given the relevance of these energy sources, there is tremendous growth in integrating Renewable Energy Resources (RESs) and Inverter-Based Resources (IBRs) into the electric power distribution network, leading to many outcomes and enhancements made possible by the operation of Distributed Generations (DGs). The DG allows electrical energy generation at distributed and individual sites, positioning better reliability, flexibility, and power quality (Aniba and Maaroufi, 2017). There have been concerns, particularly by utility companies, with possible technical challenges such as reverse power flow and over-voltage due to integrating power generated from the DGs into the existing grid. A feeder can be adequately modeled by selecting the best point of connection of a PV to accommodate the voltage drop of a shorter resistive line and to size the amount of power generation that will raise the voltage, to be consistent with the local protection relays and constraints of the substation. Both wind and PV are constrained by their intrinsic nature factors as well as extrinsic operational boundaries. These factors may cause uncertainty in the power generated from those sources.

Therefore, those considerations must be addressed to successfully interconnect the RES power to a microgrid with desired reliability and stability, contributing it to become more towards a smart grid. The main concern of distribution system operators is to keep the voltage outline within the range of standards (Gensler et al., 2016). This feature is

* Corresponding author.
E-mail address: sayawu2013@gmail.com (S.Y. Diaba).

https://doi.org/10.1016/j.egyr.2024.08.007
Received 15 July 2023; Received in revised form 22 July 2024; Accepted 4 August 2024
Available online 14 August 2024

Nomenclature

ANN	Artificial Neural Network
CO_2	Carbon Dioxide
DG	Distributed Generation
GRU	Gated Recurrent Unit
IBR	Inverter-Based Resources
IEA	International Energy Agency
LSTM	Long Short-Term Memory
MAE	Mean Absolute Error
MSE	Mean Squared Error
NIST	National Institute of Standards and Technology
NSE	Normalized Squared Error
PHANN	Physical Hybrid Artificial Neural Network
PV	Photovoltaic
PIoT	Photovoltaic Internet of Things
RES	Renewable Energy Sources
RNN	Recurrent Neural Network

achievable using modern power electronics-enabled power systems hardware, intelligent control, real-time performance, electrical circuits' instrumentation, and communication infrastructures (Luo et al., 2021; William et al., 2018). The grid's status varies spatially and temporally depending on the renewable generation variability, affecting the power quality, voltage quality, and current quality (Kroposki et al., 2010; Zhou et al., 2021). This and other technical challenges must be considered to successfully connect the RES power output, such as PV-generated output power to a smart grid.

Deep learning methods and architectures have been used in AI-based smart grid systems and have proven to be a powerful tool in terms of accuracy with respect to PV generated output power prediction. With a large dataset, deep learning methods provide accurate load forecasting, scheduling, and net-metering transaction predictions. The literature shows that deep learning can update generator and load set points depending on the load forecasts (Jones et al., 2020). Estimation algorithms for weather forecasting, natural disaster predictions, net metering, and approximate generation schedules can also be updated using deep learning algorithms. There is a trend in using deep learning for the status of power transmission lines and the prediction of faults to be managed to avoid disrupting current flow on the distribution grid (Kroposki et al., 2010). Owing to these facts, deep learning differs from traditional machine learning techniques in its ability to handle complex and high-dimensional data, capture temporal dependencies, scale with large datasets, and automate feature engineering. These capabilities make deep learning particularly well-suited for data analysis and forecasting in PV power generation, where accurate predictions of power output are essential for efficient grid integration and energy management.

A deep Recurrent Neural Network (RNN) has been proposed in (Ahn, 2021) to forecast PV power output in the short term. The various parameters of the proposed algorithm were investigated, and the study results showed that the proposed deep RNN-based short-term forecast algorithm achieved higher prediction accuracy. In (Dairi et al., 2020), the combination of deep learning algorithms, namely, AutoEncoder, Deep Belief Network, and an LSTM, was employed for renewable energy forecasting. The algorithm outperformed the standard multilayer perceptron and physical forecasting model.

The authors of (Dolara et al., 2015) employed a hybrid method consisting of a Physical Hybrid Artificial Neural Network (PHANN) based on an Artificial Neural Network (ANN) and a PV installation with clear sky theoretical line plots (solar curves). The algorithm was compared to the standard ANN method and found robust. The authors of Nabavi et al. (2021) employed a hybrid method of LSTM neural network and Discrete Wavelet Decomposition to forecast the demand and supply of energy supply. Jebli et al. (2021) studied deep learning techniques for solar energy prediction. They focused on hybrid techniques concatenating LSTM, RNN, and Gated Recurrent Unit (GRU). The proposed prediction methods revealed that the LSTM and the RNN outperform the GRU. The authors of Holmgren et al. (2017) used a forecasting module, PVLib-Python, to forecast solar power output. The accuracy of the module was examined regarding a fleet of PV power plants.

Research has proven that deep learning models enhance the accuracy of forecasts for PV power generation. As the authors of (Ahn, 2021) demonstrated that an LSTM outperformed traditional methods, achieving a Mean Absolute Error (MAE) of 12.5 kW and a Root Mean Squared Error (RMSE) of 18.3 kW. This improved accuracy facilitated better grid integration and energy management, reducing reliance on backup power sources and increasing grid stability. These improvements in forecast reliability led to more efficient energy distribution and planning, highlighting the potential of deep learning approaches in PV power generation systems.

Our paper focus on the development of a neural network-based algorithm for predicting PV-generated output power in the short term by employing a neural designer, our solution is modular and capable of being implemented in any real-life system or retrofitting any utility-based management software. To validate the model's accuracy, linear regression, and time series analysis are performed to support cross-validation. Grid operators can better coordinate control efforts and prioritize their control needs with a forecasted system state. Therefore, our deep learning-based PV forecasting system helps in increasing grid reliability, resilience, and overall system efficiency. Given the relevance of the study, there are valuable policy dimensions that are deducible from the result of the investigation.

The remainder of the paper is organized as follows: the system model is presented in Section II; data description is covered in Section III; our analysis and simulation with observed results are presented in Section IV; finally, Section V concludes our narrative.

2. System model

Consider a general input vector x, as in Eq. (1) (Xu and Liu, 2021)

$$x = [x_1, x_2, \ldots, x_n]^T \tag{1}$$

The input is processed by a type of neural network called LSTM, which is designed to work with sequential data while avoiding the issue of vanishing gradients that can occur in traditional RNNs. LSTMs have memory blocks that are connected through a series of layers (Dairi et al., 2020), and they use three gates (input, forget, and output) to regulate the flow of information within the network. LSTMs are a powerful tool for processing sequential data and have become widely used in natural language processing, speech recognition, and time series analysis.

The input is processed by an LSTM neural network, which is designed to cope with sequential data while avoiding the problem of vanishing gradients that might arise with typical RNNs. LSTMs feature memory blocks connected by a succession of layers (Dairi et al., 2020), and they manage the flow of information inside the network using three gates. They are an effective tool for processing sequential data and have found widespread application in domains such as natural language processing, speech recognition, and time series analysis. A cell, an input gate, a forget gate and an output gate, comprise the basic unit. The cell is in charge of storing the network's state across time steps, while the gates manage the flow of information into and out of the cell. The input gate controls how much fresh input is added to the cell state. It takes as inputs the current and previous hidden states and applies a *sigmoid* activation function to each, yielding a value between 0 and 1. This value is then multiplied by the candidate value, which is the result of applying the current input and the prior hidden state to a *tanh* activation function. The final product is incorporated into the cell state.

The forget gate determines how much of the previous cell state should be retained. It takes the current input and the previous hidden state as inputs and applies a *sigmoid* activation function to both, producing a value between 0 and 1. This value is then multiplied by the previous cell state, effectively "forgetting" some portion. The output gate determines how much of the cell state should be output at the current time step. It takes the current input and the previous hidden state as inputs and applies a *sigmoid* activation function to both, producing a value between 0 and 1. The current cell state is then passed through a hyperbolic tangent (tanh) activation function, and the resulting value is multiplied by the output gate value to produce the final output at the current time step. The combination of the input, forget, and output gates allows the LSTM to selectively retain or discard information across time steps, enabling it to handle long-term dependencies in sequential data better. With the three gates of the LSTM, the formulation is given in (Dolara et al., 2015; Nabavi et al., 2021), corresponding to input gate, forget gate and output gate, respectively.

The input gate

$$\gamma_i = \sigma(w_i[h_{t-1}, x_i + \beta_i]) \tag{2}$$

The forgot gate

$$\gamma_f = \sigma\left(w_i\left[h_{t-1}, x_f + \beta_f\right]\right) \tag{3}$$

The output gate

$$\gamma_o = \sigma(w_i[h_{t-1}, x_o + \beta_o]) \tag{4}$$

where γ_i, γ_f and γ_o denote the input gate, forget gate, and output gate, respectively. It is β_i, $\beta_f$and β_o corresponding to the bias of the input, forget, and output gates. The weights of the respective gates are denoted by w whilst the *sigmoid* function takes σ and is written as

$$\sigma(x) = \frac{1}{1 + e^{-1}} \tag{5}$$

The *sigmoid* is used as the recurrent activation function, and the activation function for the LSTM is a *tanh*, written as

$$\tanh = \frac{e^{2x-1}}{e^{2x+1}} \tag{6}$$

The neural network used for the predictive model has nine input features: Array 1 (W), Array 2 (W), Array 3 (W), Array 4 (W), PV Total Power (W), PV Average Power (W), Inverter Efficiency, AC total power and PV to DC Efficiency. The network architecture is shown in Figs. 1 and 2. At each iteration, the input features are passed to the input layer, which sets up the dimensions of the input sequence. The features are then processed by an LSTM layer, which is capable of handling long-term dependencies by selectively adding or subtracting features in each cell (Rosato et al., 2019; Mellit et al., 2020).

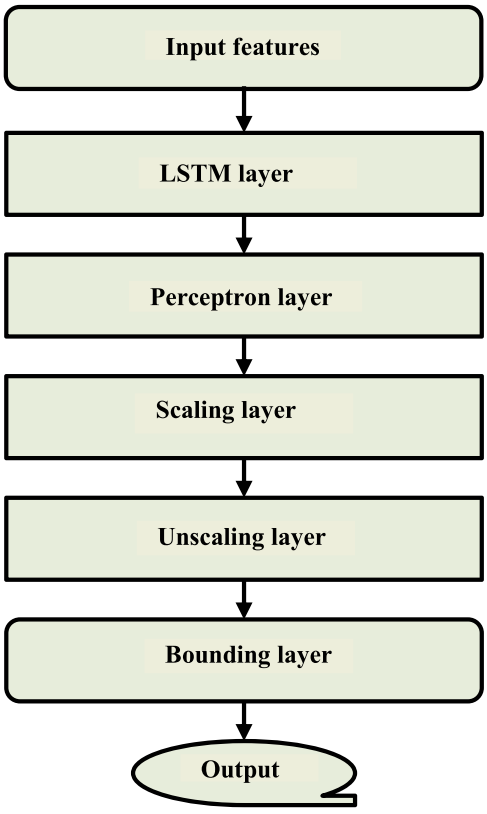

Fig. 2. The flow chart of the proposed NN model.

In our neural network architecture, the perceptron layer receives input features, which are summed with respective biases and weights. The resulting sum is then activated to produce an output forwarded to the scaling layer. The scaling layer is responsible for scaling the received features to a proper range. The scaled output features are then un-scaled by the un-scaling layer, which holds rudimentary statistics of the outputs, including the mean, standard deviation, minimum, and maximum values. Finally, the Bounding layer is used to limit the output to a specific range. Together, these layers help to ensure that the outputs are properly scaled, statistically valid, and within an appropriate range for the given task.

3. Data description

The NIST Engineering Laboratory; Energy and Environment Division captured the PV data. The dataset was captured by sensors in the second-

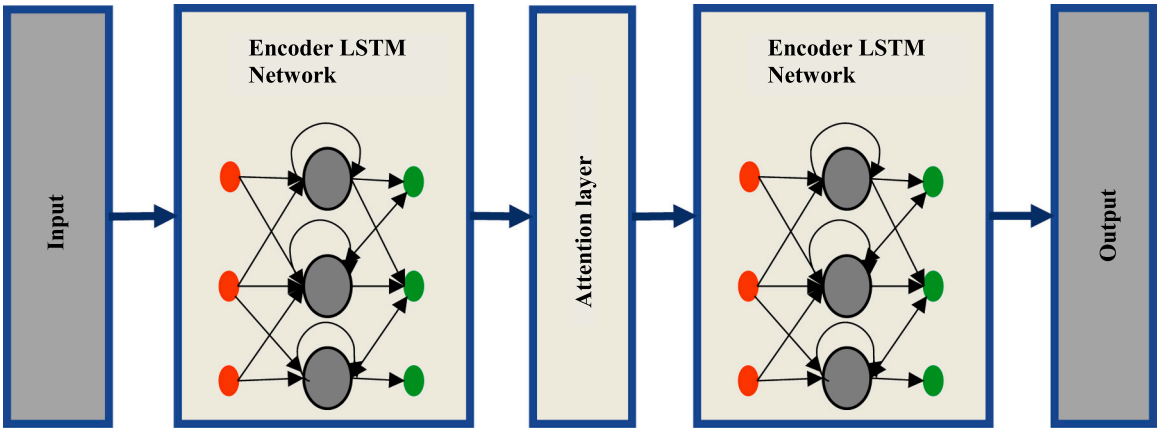

Fig. 1. Architectural description of the LSTM.

year test phase using the Net-Zero Energy Residential Test Facility. Specifically, from February 1, 2015, through January 31, 2016. The annual maximum total of minutely entries is 525600, of which 98.8 % are contained in the Net-Zero Energy Residential Test Facility second-year data (Healy et al., 2017).

Thus, the datasets can be referred to with respect to testing and standardizing modeling approaches (Boyd, 2017). This data is used for simulation analysis in this paper. The primary metadata of the dataset is presented in Table 1, while the common statistics of the measurements are shown in Table 2.

The total power from the arrays is the sum of the power from the four arrays. Thus, total power (P_t) is

$$P_t = \sum_{p=1}^{p=4} P_i \tag{7}$$

The power generated per array is determined by the product of the current (I) and the voltage (V).

$$P = I \times V \tag{8}$$

The NSE is the error measure used in this analysis. The NSE is written as

$$NSE = \frac{\sum (output - target)^2}{normalizationcoefficient} \tag{9}$$

We simulated a correlation coefficient heat map to assess the relationship between the target variable (Total AC power generated) and the other inputs. The results are presented in Table 3, and the visual representation is shown in Fig. 3. Correlation coefficients range from −1–1, where values close to 1 indicate a strong positive relationship between the input and target variables, values close to −1 indicates a strong negative relationship, and values close to 0 indicate little or no relationship between the variables. Therefore, we can use the correlation coefficient heat map to determine the degree of dependence of the target variable on the other inputs and whether a particular input significantly impacts the target variable.

The Pearson correlation coefficient r is a commonly used statistical measure in various fields such as finance, engineering, and social sciences to assess the strength of the relationship between two variables. To calculate the Pearson correlation coefficient, a formula that involves the covariance between the two variables and the standard deviation of each variable is used (Ahn, 2021).

$$r = \frac{\sum (x - x')(y - y')}{\sqrt{\sum (x - x')^2} \times \sqrt{(y - y')^2}} \tag{10}$$

where x and y denote the samples and x' and y' represent the sample means.

The MAE and Mean Squared Error (MSE) are two often used metrics in machine learning to assess the performance of a regression model. The MAE calculates the average absolute difference between the target variable's actual and projected values. It indicates how far the forecasts are from the actual values, regardless of their direction. The MSE calculates the average squared difference between the target variable's actual and anticipated values. MAE and MSE are useful for assessing a regression model's performance. While the MAE indicates the average absolute difference between the actual and projected values, the MSE indicates the error variance. A lower MAE or MSE score implies that the model performed better. They are written respectively as

$$MAE = \frac{\sum_{i=1}^{i=n} |y_i - y_{i'}|}{n} \tag{11}$$

$$MSE = \frac{1}{n} \sum_{i=1}^{i=n} (y_i - y_{i'})^2 \tag{12}$$

where n represents the number of samples y_i is the observed values and $y_{i'}$expected output.

The error statistics measure the mean, standard deviation, maximum, and minimum errors between the neural network and the testing samples in the data set. Valuable tools for testing the quality of the model are presented in the error statistics as indicated in Table 4. Table 4 below shows the mean, standard deviations, maximum, and minimum of the absolute and percentage errors of the neural network for the testing data.

Table 1
The metadata of the dataset.

Name	Description
NIST unit	Engineering Laboratory; Energy and Environment
Data format	Comma Separated Values, Images, Extensible Markup Language.
Time frame	Temporal: 2015–01–01 through 2016–12–31
Instrument	Solar, meteorological, electrical, temperature,
Spatial	Spatial: Latitude [°N], Longitude [°E], Elevation [m] Ground array: 39.1319°, −77.2141°, 138 m Roof array: 39.1354°, −77.2156°, 149 m Canopy array: 39.1385°, −77.2155°, 137 m Weather station: 39.1374°, −77.2187°, 158 m
Dictionary of data	https://www.nist.gov/file/391591

Table 2
The distributive statistics of the dataset.

Input features	Minimum	Maximum	Mean	Deviation
Array 1 (W)	−0.000113	2.76e+3	553	731
Array 2 (W)	−9.75e−5	2.7e+3	552	727
Array 3 (W)	−4.72e−6	2.71e+3	546	722
Array 4 (W)	−5.39e−5	2.75e+3	548	724
Total DC Power (W)	−2.03e−5	2.75e+3	2.2e+3	2.9e+3
Average PV Power (W)	0	6.75e+4	1.24e+4	1.65e+4
PV-DC Efficiency	−3.76e−7	0.936	0.103	0.0874
AC Total Power (W)	−64.6	1.02e+4	2.07e+3	2.76e+3
Inverter Efficiency	0	1.07	0.508	0.457

Table 3
The correlation analysis between the target and the inputs.

Input features	Correlation type	Target
Array 1 (W)	linear	0.999849
Array 2 (W)	linear	0.999889
Array 3 (W)	linear	0.999990
Array 4 (W)	linear	0.999827
Total DC Power (W)	linear	0.999918
Average PV Power (W)	linear	0.992938
Inverter Efficiency	linear	0.715417
PV to DC efficiency	linear	0.658308
AC total power (W)	linear	0.998718

4. Simulation analysis

Simulation in this paper was carried out using the neural designer on Windows 8 installed on Core i7 with a CPU of 3.4 GHz and RAM of 16 GB. The training sample is 26,783, making up 60 % of the total dataset. The selection sample is 8927, constituting 20 % of the entire dataset. It is 20 % of the gross dataset for testing samples, with a total sample of 8927. The neural network architecture was set up using the hyperparameters in Tables 5 and 6.

With the set-up parameters in Table 5, the training process is initiated. The training or learning is implemented on the neural network to achieve the best possible loss. The quasi-Newton optimization algorithm is employed. The quasi-Newton optimization algorithm is a variant of Newton's method that does not require computing the second derivatives of the objective function. Instead, the algorithm approximates

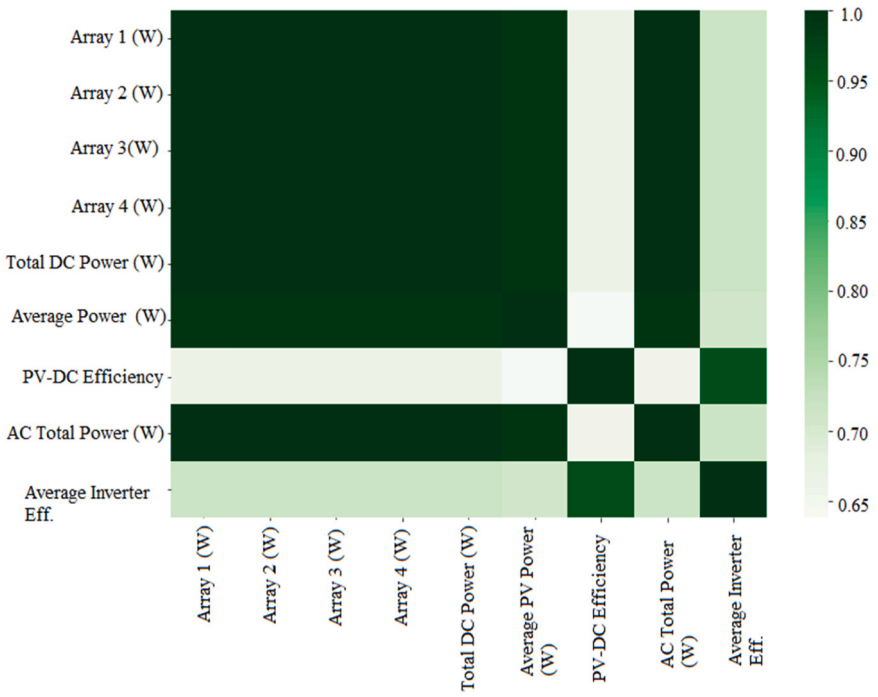

Fig. 3. The correlation coefficient heat map.

Table 4
The errors amid the neural network and the testing samples.

Error type	Minimum	Maximum	Mean	Deviation
Absolute error	0.08057	5350.14	600.026	998.4
Relative error	7.876e−6	0.5230	0.05866	0.09760
Percentage error	0.78766–3	52.3046	5.8866	9.7607

Table 5
The simulation setup parameters.

Number	Parameter	Filter / Neuron
1	LSTM	Activation/Recurrent activation
2	Activation function	Tanh / ReLu
3	Input selection	Growing input
4	Dense layer	172
5	Loss index	Normalized square error
6	Epoch	1000
7	Optimization algorithm	Quasi-Newton
8	Regularization	L2

Table 6
The training results.

Name	Value
Training error	0.00181
Selection error	0.00177
Epoch number	178
Elapse time	00:07:24
Stopping criterion	Minimum loss decreases

the inverse of the Hessian matrix using only information from the function's gradient and iteratively refines this approximation until convergence is reached. This approach can be computationally more efficient than exact Newton's method while still achieving fast convergence rates.

Fig. 4 shows the training error (blue) and selection errors (orange) during iterations. At the initial stage, the value of the training error is

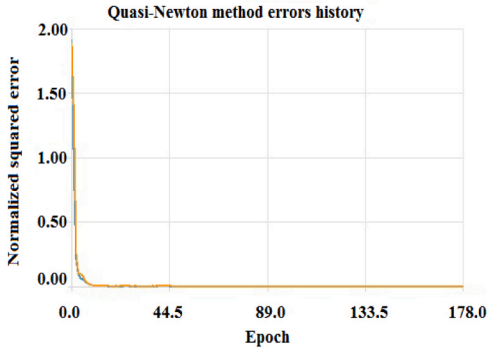

Fig. 4. Plot of the training error vs. the selection error.

1.91018, and the final value is 0.00180564 after 178 epochs. The selection error has an initial value of 1.89488 and a final value of 0.00177012 after 178 epochs.

4.1. Linear regression approach

Having determined that the correlation types between the inputs and the target are solely linear, a linear regression analysis is performed. Linear regression is a statistical approach used to model the relationship between a dependent variable and one or more independent variables. In this analysis, it has been determined that the relationship between the inputs and the target variable is solely linear, which means that a linear regression model is appropriate to test the loss of the model. The linear regression is given as (Park et al., 2020)

$$y = \beta_o + \beta_1 x_1 + \beta_2 x_2 + \ldots + \beta_n x_n + \varepsilon \tag{13}$$

where y is the dependent variable (the target), x_1, x_2, …, x_n are the independent variables (the inputs), β_0 is the intercept (the value of y when all independent variables are equal to zero), β_1, β_2, …, β_n are the coefficients (the effect of each independent variable on y), and ε is an independent error term following a normal distribution with zero mean

and σ standard deviation.

Writing Eq. (13) in its matrix notations form,

$$X = \begin{pmatrix} x_{11} & \cdots & x_{1n} \\ \vdots & \ddots & \vdots \\ x_{m1} & \cdots & x_{mn} \end{pmatrix}, Y = \begin{pmatrix} y_1 \\ \vdots \\ y_m \end{pmatrix}, \beta \begin{pmatrix} \beta_1 \\ \vdots \\ \beta_m \end{pmatrix} \tag{14}$$

Substituting Eq. (14) into Eq. (13) results

$$Y = X\beta + \varepsilon \tag{15}$$

The regressions co-efficient that minimizes the error is estimated as follows

$$\beta = \left(X^T X\right)^{-1} X^T Y \tag{16}$$

The equation of estimating the value Y the value of the regression coefficient is given as

$$Y = X\beta \tag{17}$$

In testing the loss of the model, linear regression analysis between the scaled neural network outputs and the corresponding targets for an independent testing subset are simulated. For the Total DC Power (W), the y-intercept and the slope are recorded at 645.73 and 0.88, respectively. The correlation is 0.96. The plot of the Total DC Power linear regression is shown in Fig. 5 using 8000 samples. Each circle represents a predicted value versus the actual one. The best linear fit is specified by the diagonal (black) line. This shows the scaled output within the range and outputs outside the range are not plotted, indicating a positive relationship between the two parameters.

Practically, the data present at the inverter is the most vital parameter in determining the efficiency of the inverter. The type of inverter may affect the reference level of efficiency. Therefore, technology for performance diagnosis that can accurately identify performance from the solar input energy to the system output as well as any loss and fault in the process is needed (Salcedo-Sanz et al., 2009). We cross-validate the predicted Inverter Efficiency with the real Inverter Efficiency in Fig. 6. The result provides information on Inverter Efficiency (Park et al., 2020). The result implies that the real average inverted efficiency increases with predicted average inverted efficiency, the two parameters are shown to reflect significant harmony at higher values.

The parameters for the linear regression for the output Total DC Power (W), is 161.01 for the intercept while the slope takes 0.87. The circle represents a predicted value versus the actual one. The validation between the predicted Total AC Power (W) and the real Total AC Power (W) is depicted in Fig. 7. The diagonal (black) line indicates the best linear fit, suggesting a positive association between the two parameters. The chart shows only 8000 random samples. It is worth saying that some

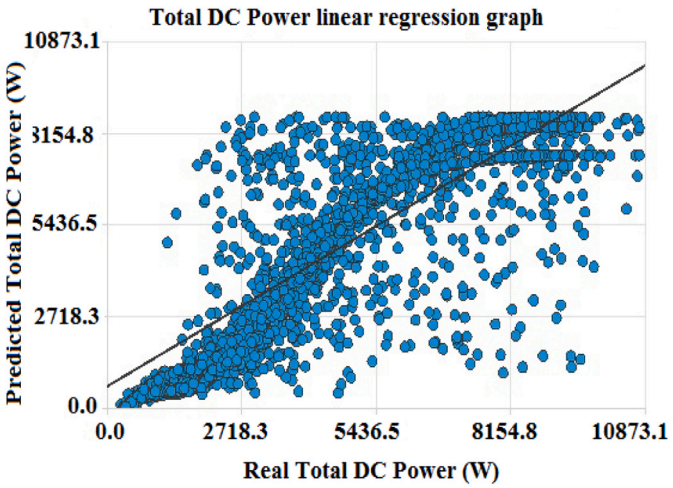

Fig. 5. Linear regression plot for Total DC Power (W).

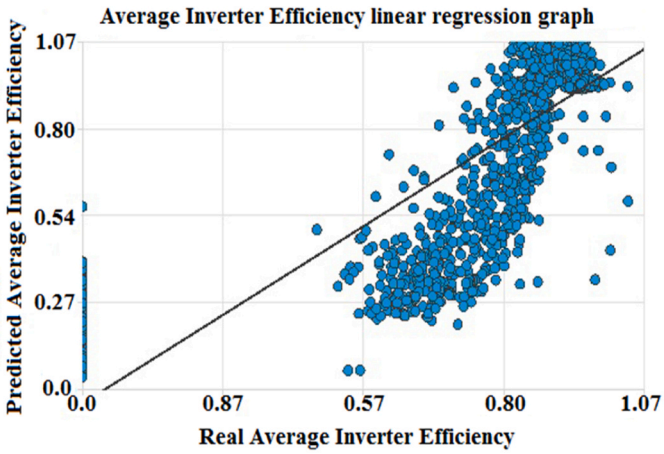

Fig. 6. Linear regression plot for Inverter Efficiency.

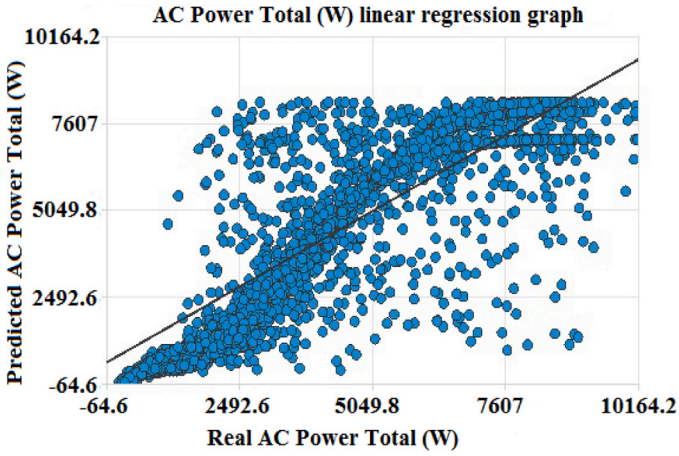

Fig. 7. Linear regression Total AC Power (W).

scaled outputs fall outside the range defined by the targets, so they are not plotted.

The primary function of the inverter is converting the DC power from the PV system to AC power that will be injected into the grid. With the deployment of power electronics, the inverter conversion rate in terms of efficiency is maximum. Higher reliability is ensured, and the operational cost is reduced (Rampinelli et al., 2014) at a higher efficiency. The inverter efficiency also depends on the level of the DC input voltage. The relationship is expected considering that the amount or estimated power of the AC is conditioned on converted estimates from the DC, irrespective of the potential power losses in the conversion process.

Fig. 8 shows the Average Inverter Efficiency versus the Total DC Power (W). According to (Rodrigo et al., 2016), the map of the efficiency of the inverter depends on the DC voltage and relative power. The Average Inverter Efficiency analysis shows that the highest efficiency is obtained at voltages of approximately 500 V, corresponding to an efficiency of approximately 99 %. The lowest efficiency is recorded at nearly 100 V, corresponding to nearly 45 % of efficiency (Rodrigo et al., 2016).

A pictorial presentation of the Average Inverter Efficiency versus the Total AC Power (W) is shown in Fig. 9. The Average Inverter Efficiency analysis shows that the inverter recorded the highest efficacy at 99 % corresponding to approximately 500 W of the total AC Power. The efficiency of the inverter remained constant after the maximum was archived, even with the increase in the AC Total Power.

To understand the visual accuracy of the model, time series plots are

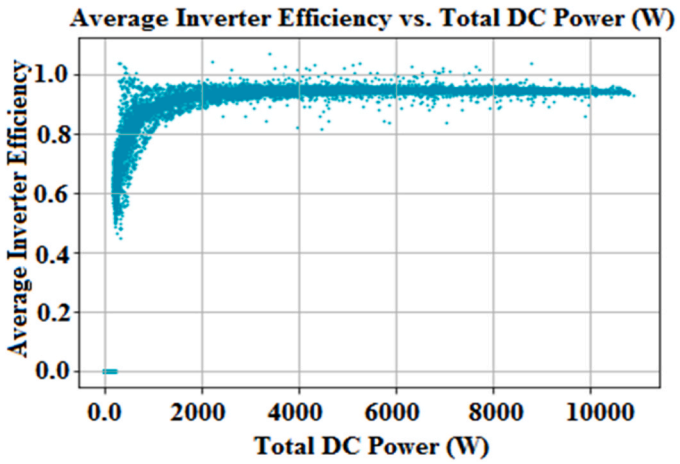

Fig. 8. Average Inverter Efficiency against Total DC Power.

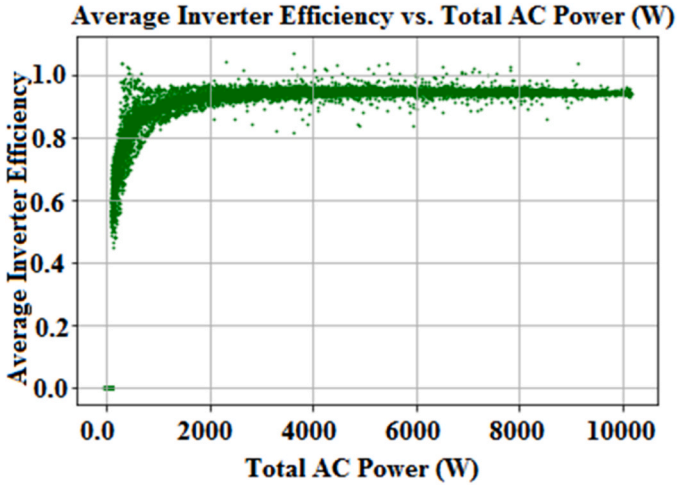

Fig. 9. Ac power total against average inverter efficiency.

plotted. This task plots the time series of both the targets in the data set and the outputs from the neural network for the testing data. It displays in the *y*-axis observations against time on the *x*-axis. The plot in Fig. 10 shows the time series of both the targets in the data set and the outputs from the neural network for the testing data. The blue line represents the target data, while the orange line represents the output data.

The plot displays the time series of the dataset's target values and the corresponding predictions generated by the neural network on the testing data. The blue line represents the target data, while the orange line represents the network's output. Visual inspection of the plot reveals that the neural network's performance surpasses the target data, indicating that the model has learned to accurately capture the underlying patterns in the data and produce high-quality predictions.

The time series of both the targets in the data set and the outputs from the neural network for the validation data are shown in Fig. 11, and it is again evident that the neural network's output has outperformed the target data. The blue line represents the target data, while the orange line represents the network's output.

Fig. 12 illustrates the time series plot of both the target values and the corresponding outputs generated by the neural network on the given dataset. The blue line indicates the target data, while the orange line shows the output from the network. The plot confirms that the neural network outperforms the target values, highlighting the potential of the proposed model for accurate estimation. This finding supports the conclusion that the model can effectively predict the accuracy of PV output, demonstrating its strong predictive capabilities in this context.

5. Conclusion

This paper proposes a deep LSTM algorithm for accurate PV power output, utilizing historical data from the NIST for short-term forecasting. To validate our approach, we compare the results of our proposed algorithm with a deep RNN model using PIoT data for short-term PV power generation forecasting, as reported in (Ahn, 2021). Our comparative analysis reveals that our proposed algorithm outperforms the deep RNN model regarding the accuracy and short-term PV power output forecasting. Based on these results, we offer useful policy suggestions for decision-makers and stakeholders in the energy industry. Our findings suggest that our proposed deep LSTM algorithm can provide more reliable and accurate forecasts of PV power output, enabling more efficient and effective management of energy resources. We believe that our research contributes to advancing the state-of-the-art in the field of PV power forecasting and can have significant implications for developing sustainable energy systems.

5.1. Policy insight

In terms of policy, the result from the study is found to be relevant for contemporary and growing energy transition issues. Considering that the benefits associated with PV power cannot be over-emphasized, an expected policy recommendation will be that more deployment of PV technology should be encouraged. However, a significant increase in the deployment of PV technology is unattainable without policy instruments such as providing more consumer- and producer-based incentives, especially for energy-related technologies. In order to promote more use

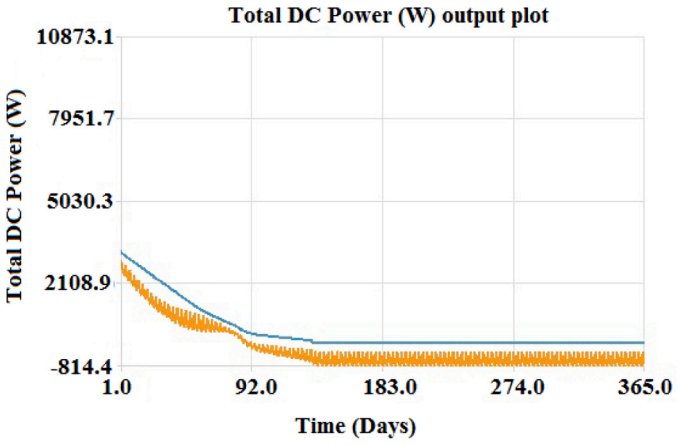

Fig. 10. Time series plot of the Total DC Power (W).

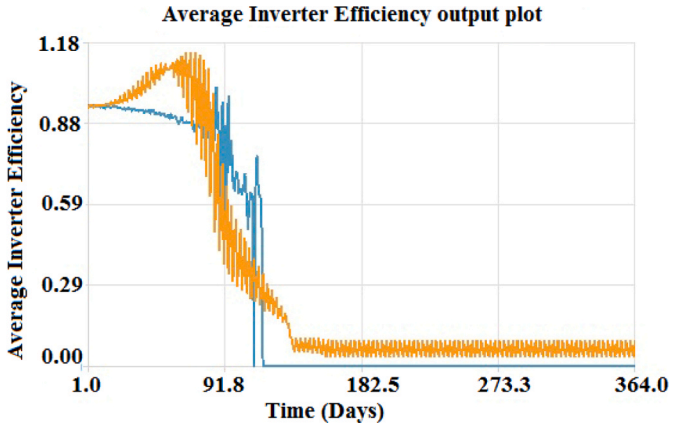

Fig. 11. Time series plot of the Average Inverter Efficiency.

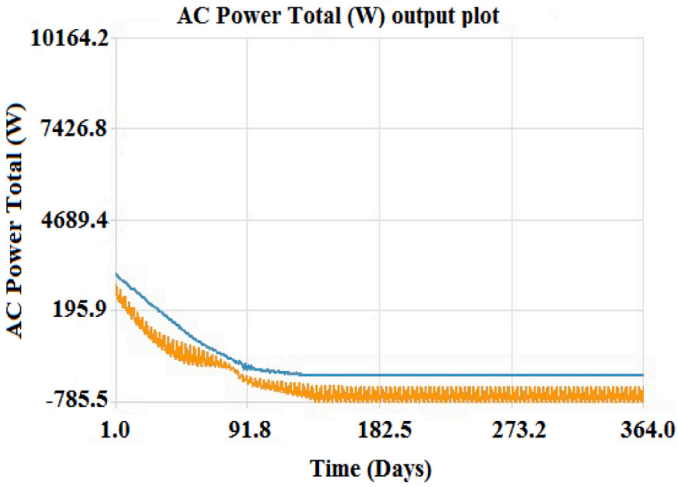

Fig. 12. Time series plot of the AC Power Total (W).

of PV power, end users such as household users could be financially incentivized by making the PV products available at a subsidized price. Moreover, reducing the cost of importation and minimizing import restrictions on energy technologies could be another effective tool for promoting PV installation and utilization. Lastly, increased investment through public-private partnership investment policy has proven to be a useful policy tool in expanding the deployment of PV installations. As evident in the report of the IEA (International Energy Agency, 2022) for the case of the United States, China, and Vietnam, the investment boom in 2020 accounted for a significant expansion in PV installations.

5.2. Study limitations and future opportunities

Having a longer period of brightness or sunlight in a Nordic country like Finland, especially during winter, is an obvious challenge. Therefore, future research endeavors could consider carrying out the experimentation during the season of long hours of brightness, otherwise, comparison experimentation could also be carried out for both Summer and Winter periods. The essence is to overcome some of the drawbacks associated with solar energy generation, such as geographic variation, latitude, and climate (Kabir et al., 2018). In the future, this study could be approached differently while guaranteeing a relevant and policy-focused result. Future work could implement the neural designer to design a model for cyber-attack detection. The focus will be on the cyber intrusion targeting prosumers injecting power into the grid. Moreover, the study methodology could be improved by incorporating more statistical and/or econometric dimensions, especially when using compatible time series datasets. Future studies could consider similar cases for cross-sectional households in the same or different geographical locations along the time series dataset. More importantly, a regime-switching approach such as the Markov switching methodology could provide different observations for different scenarios, which applies to the case under consideration. Hybrid models, deployed on edge devices integrated with IoT sensors, will be a future trend, enabling immediate responses to weather changes and enhancing grid stability. Also, deep learning will play a crucial role in predictive maintenance and fault detection.

Authors statement

The authors equally contributed to all aspects of this manuscript, including study conception and design, data collection, data analysis, interpretation of results, and manuscript preparation.

CRediT authorship contribution statement

Andrew Alola: Validation, Supervision. **Sayawu Diaba:** Writing – original draft, Visualization, Software, Methodology, Conceptualization. **Mohammed Elmusrati:** Writing – review & editing, Supervision. **Marcelo Simoes:** Writing – review & editing, Supervision.

Declaration of Competing Interest

The authors declare that they have no known competing financial interests or personal relationships that could have appeared to influence the work reported in this paper.

Data Availability

Data will be made available on request.

References

Ahn, H.K., Park, N, 2021. Deep RNN-based photovoltaic power short-term forecast using power IoT Sensors. *Energies* 14 no. 2, 436. https://doi.org/10.3390/en14020436.

B.G. Aniba and M. Maaroufi, "Impact of load and renewable energy uncertainties on single and multiple energy storage systems sizing," 2017 IEEE Power & Energy Society Innovative Smart Grid Technologies Conference (ISGT), 2017, pp. 1-5, doi: 10.1109/ISGT.2017.8086031.

Boyd, M., 2017. Performance Data from the NIST Photovoltaic Arrays and Weather Station. J. Res. Natl. Inst. Stand. Technol. Volume 122, 40. https://doi.org/10.6028/jres.122.040.

Dairi, A., Harrou, F., Sun, Y., Khadraoui, S., 2020. Short-term forecasting of photovoltaic solar power production using variational auto-encoder driven deep learning approach. Appl. Sci.

Dolara, A., Grimaccia, F., Leva, S., Mussetta, M., Ogliari, E., 2015. A physical hybrid artificial neural network for short term forecasting of PV plant power output. Energies 8 (2), 1138–1153.

Gensler, A., Henze, J., Sick, B., Raabe, N., 2016. Deep Learning for solar power forecasting - an approach using AutoEncoder and LSTM NeuralNetworks. IEEE Int. Conf. Syst. Man, Cybern. (SMC) 2016, 002858–002865. https://doi.org/10.1109/SMC.2016.7844673.

Healy, W.M., Fanney, A.H., Dougherty, B.P., Ng, L., Payne, V., Ullah, T., Omar, F., 2017. Performance data from the NIST net-zero energy residential test facility. J. Res. Natl. Inst. Stand. Technol. Volume 122, 14. https://doi.org/10.6028/jres.122.014.

Holmgren, W.F., Lorenzo, A.T., Hansen, C., 2017. A comparison of PV power forecasts using PVLib-python. IEEE 44th Photovolt. Spec. Conf. (PVSC) 2017, 1127–1131. https://doi.org/10.1109/PVSC.2017.8366724.

International Energy Agency (2022). Solar PV. ⟨https://www.iea.org/reports/solar-pv⟩. (Accessed June 3, 2022).

I. Jebli, F. Belouadha, M.I. Kabbaj, A. Tilioua, "Deep Learning based Models for Solar Energy Prediction," 2021 *Advances in Science, Technology and Engineering Systems Journal* Vol. 6, No. 1, 349-355 (2021).

Jones, C.B., Chavez, A.R., Darbali-Zamora, R., Hossain-McKenzie, S., 2020. Implementation of intrusion detection methods for distributed photovoltaic inverters at the grid-edge. IEEE Power Energy Soc. Innov. Smart Grid Technol. Conf. (ISGT) 1–5. https://doi.org/10.1109/ISGT45199.2020.9087756.

E. Kabir, P. Kumar, S. Kumar, A.A. Adelodun, K. H, "Solar energy: Potential and future prospects," Renewable and Sustainable Energy Reviews, 82, 894-900, 2018.

B. Kroposki, C. Pink, R. DeBlasio, H. Thomas, M. Simões, and P.K. Sen, "Benefits of Power Electronic Interfaces for Distributed Energy Systems," *IEEE Trans. Energy Convers.*, vol. 25, no. 3, pp. 901–908, Sep. 2010, doi: 10.1109/TEC.2010.2053975.

Kruitwagen, L., Story, K.T., Friedrich, J., 2021. A global inventory of photovoltaic solar energy generating units. Nature 598, 604–610. https://doi.org/10.1038/s41586-021-03957-7.

X. Luo, D. Zhang, X. Zhu, "Deep learning-based forecasting of photovoltaic power generation by incorporating domain knowledge," 2021 *Energy*. Volume 225, June 15 2021, 120240.

Mellit, A., Pavan, A.M., Ogliari, E., Leva, S., Lughi, V., 2020. Advanced methods for photovoltaic output power forecasting: a review. Appl. Sci. 10, 487. https://doi.org/10.3390/app10020487.

Nabavi, S.A., Motlagh, N.H., Zaidan, M.A., Aslani, A., Zakeri, B., 2021. Deep learning in energy modeling: application in smart buildings with distributed energy generation. IEEE Access vol. 9, 125439–125461. https://doi.org/10.1109/ACCESS.2021.3110960.

Park, C.Y., Hong, S.H., Lim, S.C., Song, B.C., Park, S.W., Huh, J.H., Kim, J.C., 2020. Inverter efficiency analysis model based on solar power estimation using solar radiation. Processes 8, 1225. https://doi.org/10.3390/pr8101225.

Rampinelli, G.A., Krenzinger, A., Romero, F.C., June 2014. Mathematical models for efficiency of inverters used in grid connected photovoltaic systems. Renew. Sustain. Energy Rev. Volume 34, 578–587.

Rodrigo, P.M., Velázquez, R., Fernández, E.F., 2016. DC/AC conversion efficiency of grid-connected photovoltaic inverters in central Mexico. Sol. Energy Volume 139, 650–665. December 1.

Rosato, A., Panella, M., Araneo, R., Andreotti, A., 2019. A neural network based prediction system of distributed generation for the management of microgrids. IEEE Trans. Ind. Appl. vol. 55 (6), 7092–7102. https://doi.org/10.1109/TIA.2019.2916758.

Salcedo-Sanz, S., Pérez-Bellido, A.M., García, E.G.O., Figueras, A.P., Correoso, P.L.F., 2009. Accurate short-term wind speed forecasting by exploiting diversity in input data using banks of artificial neural networks. Neurocomputing 72, 1336–1341.

H. William, T.H. Chen, B. Dougherty, A.H. Fanney, T. Ullah, W.V. Payne, L. Ng, F. Omar. "Net Zero Energy Residential Test Facility Instrumented Data; 2018 1," October 2018. doi: ⟨https://doi.org/10.18434/T4/1503134⟩.

B. Xu, J. Liu, "False Data Detection Based on LSTM network in Smart Grid," 2021 *4th International Conference on Advanced Electronic Materials, Computers and Software Engineering* (AEMCSE).

H. Zhou, Q. Liu, K. Yan, Y. Du. "Deep Learning Enhanced Solar Energy Forecasting with AI Driven IoT," 2021 Hindawi Wireless Communications and Mobile Computing. Volume 2021, Article ID 9249387, 11 pages.